Inorganic Chemistry
Cite This: Inorg. Chem. XXXX, XXX, XXX−XXX
Article
pubs.acs.org/IC

Impact of Benzannulation Site at the Diimine (N^N) Ligand on the Excited-State Properties and Reverse Saturable Absorption of Biscyclometalated Iridium(III) Complexes

Bingqing Liu,[†] Levi Lystrom,[†] Samuel L. Brown,[‡] Erik K. Hobbie,[‡] Svetlana Kilina,[†] and Wenfang Sun*,[†]

[†]Department of Chemistry and Biochemistry, North Dakota State University, Fargo, North Dakota 58108-6050, United States
[‡]Materials and Nanotechnology Program, North Dakota State University, Fargo, North Dakota 58108-6050, United States

Supporting Information

ABSTRACT: Ten biscyclometalated monocationic Ir(III) complexes were synthesized and studied to elucidate the effects of extending π-conjugation of the diimine ligand (N^N = 2,2′-bipyridine in **Ir1**, 2-(pyridin-2-yl)quinoline in **Ir2**, 2-(pyridin-2-yl)[6,7]benzoquinoline in **Ir3**, 2-(pyridin-2-yl)-[7,8]benzoquinoline in **Ir4**, phenanthroline in **Ir5**, benzo[*f*]-[1,10]phenanthroline in **Ir6**, naphtho[2,3-*f*][1,10]-phenanthroline in **Ir7**, 2,2′-bisquinoline in **Ir8**, 3,3′-biisoquinoline in **Ir9**, and 1,1′-biisoquinoline in **Ir10**) via benzannulation at 2,2′-bipyridine on the excited-state properties and reverse saturable absorption (RSA) of these complexes. Either a bathochromic or a hypsochromic shift of the charge-transfer absorption band and emission spectrum was observed depending on the benzannulation site at the 2,2′-bipyridine ligand. Benzannulation at the 3,4-/3′,4′-position or 5,6-/5′,6′-position of 2,2′-bipyridine ligand or at the 6,7-position of the quinoline ring on the N^N ligand caused red-shifted charge-transfer absorption band and emission band for complexes **Ir2**, **Ir8**, **Ir10** vs **Ir1** and **Ir3** vs **Ir2**, while benzannulation at the 4,5-/4′,5′-position of 2,2′-bipyridine ligand or at the 7,8-position of the quinoline ring on the N^N ligand induced a blue shift of the charge-transfer absorption and emission bands for complex **Ir9** vs **Ir1** and **Ir4** vs **Ir2**. However, benzannulation at the 2,2′,3,3′-position of 2,2′-bipyridine or 5,6-position of phenanthroline ligand had no impact on the energy of the charge-transfer absorption band and emission band of complexes **Ir5**−**Ir7** compared with those of **Ir1**. The observed phenomenon was explained by the frontier molecular orbital (FMO) symmetry analysis. Site-dependent benzannulation also impacted the spectral feature and intensity of the triplet transient absorption spectra and lifetimes drastically. Consequently, the RSA strength of these complexes varied with a trend of **Ir7** > **Ir5** ≈ **Ir6** ≈ **Ir1** > **Ir3** > **Ir2** > **Ir10** > **Ir4** > **Ir8** > **Ir9** at 532 nm for 4.1 ns laser pulses.

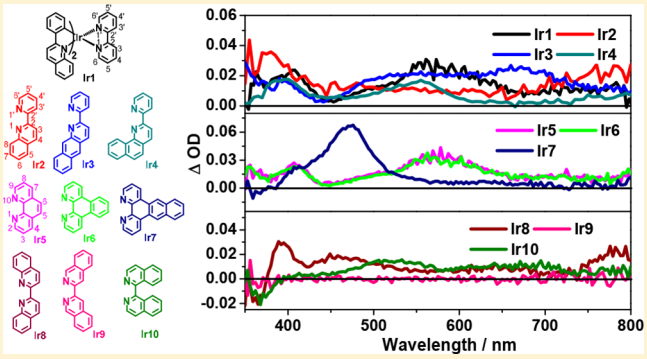

INTRODUCTION

Among the diverse transition-metal complexes, pseudo-octahedral d^6 iridium(III) complexes have attracted growing interest in both academia and industry during the past two decades.[1−4] The strong spin−orbit coupling induced by the Ir(III) ion enhances the intersystem crossing (ISC) rate and promotes triplet excited-state formation. These characteristics spark research interest in exploring potential binding geometries with novel ancillary ligands. After the seminal work by Watts et al. on triply ortho-metalated Ir(III) complexes in the 1980s,[5] diverse mono-, bis-, and triscyclometalated complexes with different polypyridine ligands or cyclometalating ligands have been reported.[6,7] Among these complexes, biscyclometalated monocationic Ir(III) complexes are discovered to play a crucial role in various applications, such as sensitized photo-upconversion,[3] organic light emitting diodes (OLEDs),[8−11] light-emitting electrochemical cells (LEECs),[12,13] photodynamic therapy,[14−16] nonlinear optics,[17−19] photocatalysis,[20−22] and bioimaging and biosensing.[23]

In light of the structures of the monocationic Ir(III) complexes $[(N^N)Ir(C^N)_2]^+$ (where N^N refers to the diimine ligand and C^N refers to the cyclometalating ligand), the combination of one N^N ligand and two identical C^N ligands provides the opportunity to control the photophysical properties of these complexes via a diverse selection and combination of ligands. Generally, the electron-deficient N^N ligand is the major contributor to the lowest unoccupied molecular orbital (LUMO) in these Ir(III) complexes, while the C^N ligands and the d-orbital of the Ir(III) ion hold the majority of the highest occupied molecular orbital (HOMO).[24−26] Consequently, extending π-conjugation or introducing electron-donating or withdrawing substituents on the N^N ligand

Received: November 10, 2018

DOI: 10.1021/acs.inorgchem.8b03162
Inorg. Chem. XXXX, XXX, XXX−XXX

would alter the LUMO exclusively. It has been reported that incorporation of electron-donating substituents, such as an amino or methoxy group, to the N^N ligand raised the LUMO and blue-shifted the low-energy absorption bands of Ir(III) complexes. In contrast, Ir(III) complexes bearing electron-withdrawing substituents at the N^N ligand, such as fluoro or cyano, displayed red-shifted low-energy absorption bands due to the stabilized LUMOs.[26,27] Another approach to tune the LUMO energy is to incorporate π-conjugated units to the N^N ligand by benzannulation. It was reported that the energy of the LUMO decreased from −3.15 eV to −3.38 eV for the Ir(III) complex bearing 2-(pyridin-2-yl)quinoline ligand upon benzannulation at the 2,2′-bipyridine ligand.[26] Additionally, expanding π-conjugation of the N^N ligand via benzannulation or incorporation of π-conjugated substituents simultaneously induces more $^3\pi,\pi^*$ character into the lowest triplet excited state (T_1).[17,28−33] In contrast to the charge-transfer-based T_1 state (^{3}CT), the $^3\pi,\pi^*$-based T_1 state typically exhibits a longer lifetime, structured emission bands, and a higher emission quantum yield. Therefore, extending π-conjugation on the N^N ligand can serve as an adjuster for both the lowest singlet and triplet excited states.

In the reported work on benzannulation on organic compounds, either hypsochromic or bathochromic shifts in the absorption and emission spectra have been observed relying on the benzannulation site.[34−37] Despite finding this unusual phenomenon in small organic molecules, examples featuring the impacts of varied benzannulation site at the ligands on organometallic complexes are still rare.[32,38] In seeking a better understanding of the influences of benzannulation site at the ligands on the photophysical properties of the complexes, the seminal report by Thompson and Gordon[38] on the (N^N^N)-PtCl derivatives has intrigued our interest in other heavy transition-metal complexes, such as the Ir(III) complexes. In our previous work, we explored a series of cyclometalated monocationic Ir(III) complexes employing 1,2-diphenyl-9*H*-pyreno[4,5-*d*]imidazole as the C^N ligands, and 2-(pyridin-2-yl)quinoline and its derivatives as the N^N ligand.[32] In comparison to the parent complex bearing the 2-(pyridin-2-yl)quinoline ligand, pronounced red- or blue-shift in the absorption and emission spectra was observed relying on the site-selective benzannulation at the N^N ligand. This effect was explained by analyzing the frontier molecular orbitals symmetry at the benzannulation site of the parent complex via theoretical calculations. While this phenomenon has been well explained for our previously studied complexes, validation of the prediction from our aforementioned work on controlling the ground- and excited-state properties of the Ir(III) complexes via benzannulation at the previously undeveloped sites of N^N ligand is still needed. Moreover, because of their readily adjustable ground- and triplet excited-state absorption, these complexes have the potential for use as reverse saturable absorbers, which is worthy of an in-depth study.[17−19,29−31,33,39−42]

Targeting these goals, we have synthesized 10 biscyclometalated Ir(III) complexes (Chart 1), in which 2-phenylquinoline was utilized as the cyclometalating ligands and 2,2′-bipyridine (bpy) derivatives with varied π-conjugation were used as the N^N ligand. Extending π-conjugation of the bpy ligand was realized via benzannulation at one pyridine ring (**Ir2**−**Ir4**), at the bridge of the two pyridine rings (**Ir5**−**Ir7**), or at the different sites (i.e., 5,6-/5′,6′-, 4,5-/4′,5′-, or 3,4-/3′,4′-) of both pyridine rings (**Ir8**−**Ir10**). Complexes **Ir2**−**Ir4**, **Ir6**, **Ir7**, **Ir9**, and **Ir10** are new complexes that are first reported herein. Although

Chart 1. Structures of Biscyclometalated Ir(III) Complexes Ir1−Ir10

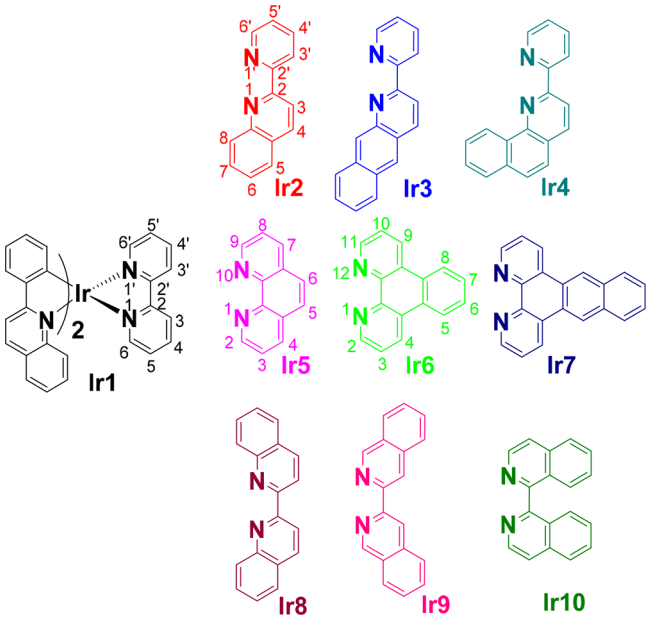

complexes **Ir1**,[43] **Ir5**[44] and **Ir8**[45] are known in the literature, previous work has focused on their biological/biomedical activities, and no systematic photophysical or reverse saturable absorption (RSA) studies have been reported for these complexes. More importantly, these complexes fall naturally into our focus on a comprehensive understanding of the impact of benzannulation site at the N^N ligand on the ground- and excited-state properties and RSA of the biscyclometalated Ir(III) complexes.

EXPERIMENTAL SECTION

Materials and Synthesis. All reagents and solvents were purchased from Alfa Aesar or VWR International and used as is unless otherwise noted. Al_2O_3 gels (activated, neutral) and silica gels (230−400 mesh) for column chromatography were purchased from Sorbent Technology. The N^N ligands 2,2′-bipyridine (**L1**), phenanthroline (**L5**), and 2,2′-bisquinoline (**L8**) were purchased from Alfa Aesar. The synthesis of 2-(pyridin-2-yl)quinoline (**L2**),[46] 2-(pyridin-2-yl)[6,7]-benzoquinoline (**L3**),[47] 2-(pyridin-2-yl)[7,8]benzoquinoline (**L4**),[48] benzo[*f*][1,10]phenanthroline (**L6**),[49] naphtho[2,3-*f*][1,10]-phenanthroline (**L7**),[50] 3,3′-biisoquinoline (**L9**),[51] and 1,1′-biisoquinoline (**L10**)[51,52] followed the published procedures. 2-Phenylquinoline (C^N ligand) and its Ir(III) dimer $[Ir(C^N)_2Cl]_2$ were prepared following reported procedures.[53] ^{1}H NMR spectroscopy, high-resolution mass spectrometry (HRMS), and elemental analyses were applied to characterize these complexes. ^{1}H NMR spectra were measured on a Varian Oxford 400 or Bruker 400 spectrometer in $CDCl_3$ or d_6-DMSO using tetramethylsilane (TMS) as the internal standard. A Bruker BioTOF III mass spectrometer was used for ESI-HRMS analyses. Elemental analyses were conducted by NuMega Resonance Laboratories, Inc. in San Diego, California.

General Procedure for the Synthesis of Ir1−Ir10. The Ir(III) dimer $[Ir(C^N)_2Cl]_2$ (0.03 mmol), N^N ligand (0.06 mmol), and $AgSO_3CF_3$ (0.06 mmol) were added in CH_2Cl_2 and MeOH (v/v = 2:1, 30 mL). The mixture was purged with nitrogen and brought to reflux for 24 h without light illumination. After the reaction was completed, the mixture was cooled to room temperature, and NH_4PF_6 (0.3 mmol) was added and kept stirring at r.t. for 2 h. Then, removal of the solvent and purification of the crude product by column chromatography (neutral alumina gel, dichloromethane/hexane (3:1−1:0, v/v)) afforded the target Ir(III) complexes.

DOI: 10.1021/acs.inorgchem.8b03162
Inorg. Chem. XXXX, XXX, XXX−XXX

Complex ***Ir1***. The obtained product was an orange solid (36 mg, yield: 66%). ^{1}H NMR (400 MHz, $CDCl_3$): δ 8.27 (d, J = 8.3 Hz, 2H), 8.23−8.07 (m, 6H), 8.05−7.91 (m, 4H), 7.71 (dd, J = 8.1, 1.4 Hz, 2H), 7.43−7.32 (m, 4H), 7.25 (d, 2H), 7.20−7.13 (m, 2H), 6.99 (ddd, J = 8.7, 6.1, 1.5 Hz, 2H), 6.86−6.79 (m, 2H), 6.55 (dd, J = 7.7, 0.7 Hz, 2H). ESI−HRMS (m/z): calcd. for $[C_{40}H_{28}N_4Ir]^+$, 757.1943; found, 757.1955. Anal. Calcd (%) for $C_{40}H_{28}F_6IrN_4P$: C, 53.27; H, 3.13; N, 6.21. Found: C, 53.59; H, 3.48; N, 5.99.

Complex ***Ir2***. The product obtained was an orange solid (31 mg, yield: 54%). ^{1}H NMR (400 MHz, $CDCl_3$) δ 8.46−8.37 (m, 2H), 8.37−8.21 (m, 3H), 8.18−8.10 (m, 1H), 8.09−8.00 (m, 2H), 7.84 (dd, J = 7.8, 4.2 Hz, 2H), 7.79 (d, J = 7.2 Hz, 1H), 7.61 (dd, J = 15.7, 7.9 Hz, 3H), 7.51 (dd, J = 14.7, 8.3 Hz, 2H), 7.45−7.35 (m, 3H), 7.25 (s, 1H), 7.16 (ddd, J = 15.8, 12.3, 4.7 Hz, 3H), 7.08 (t, J = 7.1 Hz, 1H), 7.02−6.80 (m, 4H), 6.54 (d, J = 7.2 Hz, 1H), 6.34 (d, J = 7.4 Hz, 1H). ESI−HRMS (m/z): calcd. for $[C_{44}H_{30}N_4Ir]^+$, 807.2100; found, 807.2136. Anal. Calcd (%) for $C_{44}H_{30}F_6IrN_4P{\cdot}0.3C_6H_{14}$ (C_6H_{14}: hexane): C, 56.50; H, 3.64; N, 5.68. Found: C, 56.63; H, 3.26; N, 5.46.

Complex ***Ir3***. The obtained product was an orange solid (34 mg, yield: 57%). ^{1}H NMR (400 MHz, d_6−DMSO): δ 8.72 (dt, J = 9.0, 6.9 Hz, 3H), 8.67 (s, 1H), 8.38 (d, J = 7.0 Hz, 1H), 8.28 (t, J = 8.0 Hz, 2H), 8.21−8.09 (m, 4H), 8.06 (ddd, J = 9.3, 7.1, 1.2 Hz, 2H), 7.86 (dd, J = 7.7, 0.8 Hz, 1H), 7.82−7.70 (m, 3H), 7.66−7.62 (m, 1H), 7.58−7.52 (m, 1H), 7.45−7.35 (m, 2H), 7.24−7.15 (m, 2H), 7.08−6.95 (m, 3H), 6.87 (ddd, J = 15.5, 12.7, 5.3 Hz, 4H), 6.38 (dd, J = 10.8, 7.7 Hz, 2H). ESI−HRMS (m/z): calcd. for $[C_{48}H_{32}N_4Ir]^+$, 857.2256; found, 857.2241. Anal. Calcd for $C_{48}H_{32}F_6IrN_4P{\cdot}0.9CH_2Cl_2$: C, 54.46; H, 3.16; N, 5.20. Found: C, 54.20; H, 3.15; N, 5.39.

Complex ***Ir4***. The obtained product was an orange solid (52 mg, yield: 87%). ^{1}H NMR (400 MHz, $CDCl_3$): δ 9.22 (d, J = 8.8 Hz, 1H), 8.63 (d, J = 8.2 Hz, 1H), 8.52 (d, J = 8.6 Hz, 1H), 8.43 (d, J = 8.9 Hz, 1H), 8.31 (d, J = 8.2 Hz, 1H), 8.13 (t, J = 7.8 Hz, 1H), 8.05 (d, J = 6.8 Hz, 1H), 7.93 (dd, J = 10.4, 8.1 Hz, 3H), 7.84 (d, J = 8.7 Hz, 1H), 7.69−7.58 (m, 3H), 7.48 (dt, J = 9.5, 6.9 Hz, 3H), 7.34−7.21 (m, 4H), 7.14−6.99 (m, 3H), 6.77 (d, J = 8.7 Hz, 1H), 6.68 (t, J = 7.5 Hz, 1H), 6.64−6.54 (m, 2H), 6.50 (t, J = 7.2 Hz, 2H), 6.32 (t, J = 7.6 Hz, 1H), 6.12 (d, J = 8.1 Hz, 1H). ESI−HRMS (m/z): calcd. for $[C_{48}H_{32}N_4Ir]^+$, 857.2256; found, 857.2289. Anal. Calcd for $C_{48}H_{32}F_6IrN_4P{\cdot}0.5CH_2Cl_2$: C, 55.77; H, 3.18; N, 5.36. Found: C, 55.37; H, 3.32; N, 5.36.

Complex ***Ir5***. The obtained product was an orange solid (32 mg, yield: 58%). ^{1}H NMR (400 MHz, d_6−DMSO) δ 8.74 (dd, J = 8.2, 1.4 Hz, 2H), 8.60 (d, J = 9.0 Hz, 2H), 8.51−8.45 (m, 4H), 8.36 (d, J = 7.3 Hz, 2H), 8.09 (s, 2H), 8.05 (dd, J = 8.2, 5.2 Hz, 2H), 7.81 (dd, J = 8.1, 1.3 Hz, 2H), 7.23 (ddd, J = 15.0, 8.0, 1.0 Hz, 4H), 7.11 (d, J = 9.0 Hz, 2H), 6.91−6.78 (m, 4H), 6.54 (dd, J = 7.7, 0.8 Hz, 2H). ESI−HRMS (m/z): calcd. for $[C_{42}H_{28}N_4Ir]^+$, 781.1943; found, 781.1966. Anal. Calcd for $C_{42}H_{28}F_6IrN_4P$: C, 54.48; H, 3.05; N, 6.05. Found: C, 54.25; H, 2.98; N, 6.02.

Complex ***Ir6***. The obtained product was an orange solid (41 mg, yield: 70%). ^{1}H NMR (400 MHz, $CDCl_3$) δ 9.04 (d, J = 8.1 Hz, 2H), 8.51−8.43 (m, 4H), 8.20 (d, J = 8.9 Hz, 2H), 8.16 (d, J = 8.6 Hz, 2H), 8.06 (d, J = 8.0 Hz, 2H), 7.88 (dd, J = 8.4, 5.2 Hz, 2H), 7.59−7.51 (m, 4H), 7.23−7.05 (m, 6H), 6.83 (td, J = 7.5, 1.3 Hz, 2H), 6.76 (ddd, J = 8.6, 6.9, 1.4 Hz, 2H), 6.66−6.55 (m, 2H). ESI−HRMS (m/z): calcd. for $[C_{46}H_{30}N_4Ir]^+$, 831.2100; found, 831.2123. Anal. Calcd for $C_{46}H_{30}F_6IrN_4P{\cdot}0.5C_6H_{14}{\cdot}2H_2O$ (C_6H_{14}: hexane): C, 55.78; H, 3.92; N, 5.31. Found: C, 55.70; H, 4.20; N, 5.64.

Complex ***Ir7***. The obtained product was an orange solid (51 mg, yield: 83%). ^{1}H NMR (400 MHz, d_6−DMSO) δ 9.57−9.46 (m, 4H), 8.63 (d, J = 9.0 Hz, 2H), 8.53 (d, J = 8.7 Hz, 2H), 8.42−8.32 (m, 4H), 8.20 (dd, J = 6.3, 3.3 Hz, 2H), 8.10 (dd, J = 8.4, 5.2 Hz, 2H), 7.83 (dd, J = 8.1, 1.2 Hz, 2H), 7.76 (dd, J = 6.4, 3.2 Hz, 2H), 7.22 (ddd, J = 8.8, 7.4, 6.3 Hz, 6H), 6.96−6.85 (m, 4H), 6.54−6.48 (m, 2H). ESI−HRMS (m/z): calcd. for $[C_{50}H_{32}N_4Ir]^+$, 881.2256; found, 881.2291. Anal. Calcd for $C_{50}H_{32}F_6IrN_4P{\cdot}0.3CH_2Cl_2$: C, 57.46; H, 3.13; N, 5.33. Found: C, 57.37; H, 3.07; N, 5.37.

Complex ***Ir8***. The obtained product was a red solid (38 mg, yield: 63%). ^{1}H NMR (400 MHz, d_6−DMSO) δ 8.72 (d, J = 8.6 Hz, 2H), 8.50 (d, J = 8.7 Hz, 2H), 8.32 (d, J = 8.8 Hz, 2H), 8.22 (d, J = 9.0 Hz, 2H), 8.11−8.03 (m, 2H), 8.01−7.88 (m, 4H), 7.60−7.49 (m, 4H), 7.47−7.35 (m, 4H), 7.10 (ddd, J = 8.6, 6.9, 1.4 Hz, 2H), 7.06−6.98 (m, 2H), 6.89−6.79 (m, 4H), 6.36−6.28 (m, 2H). ESI−HRMS (m/z): calcd. for $[C_{48}H_{32}N_4Ir]^+$, 857.2256; found, 857.2233. Anal. Calcd for $C_{48}H_{32}F_6IrN_4P{\cdot}1.1CH_2Cl_2$: C, 53.84; H, 3.15; N, 5.11. Found: C, 53.94; H, 2.95; N, 5.13.

Complex ***Ir9***. The obtained product was an orange solid (20 mg, yield: 33%). ^{1}H NMR (400 MHz, d_6−DMSO) δ 9.49 (s, 2H), 9.13 (d, J = 8.9 Hz, 2H), 8.68 (d, J = 8.7 Hz, 2H), 8.54 (s, 2H), 8.46 (d, J = 9.0 Hz, 2H), 8.30 (s, 2H), 8.16 (d, J = 8.2 Hz, 2H), 7.96 (d, J = 7.9 Hz, 2H), 7.86 (d, J = 7.3 Hz, 2H), 7.78−7.66 (m, 6H), 7.27 (s, 2H), 6.87 (s, 2H), 6.58−6.52 (m, 2H), 6.03 (d, J = 7.8 Hz, 2H). ESI−HRMS (m/z): calcd. for $[C_{48}H_{32}N_4Ir]^+$, 857.2256; found, 857.2241. Anal. Calcd for $C_{48}H_{32}F_6IrN_4P{\cdot}0.2C_6H_{14}$ (C_6H_{14}: hexane): C, 57.98; H, 3.44; N, 5.50. Found: C, 58.00; H, 3.58; N, 5.20.

Complex ***Ir10***. The obtained product was a red solid (34 mg, yield: 56%). ^{1}H NMR (500 MHz, d_6−DMSO) δ 8.52 (d, J = 9.0 Hz, 2H), 8.44 (d, J = 8.8 Hz, 2H), 8.26 (d, J = 8.2 Hz, 2H), 8.03 (dt, J = 14.1, 5.9 Hz, 8H), 7.82−7.76 (m, 2H), 7.72 (d, J = 8.0 Hz, 2H), 7.48 (d, J = 6.3 Hz, 4H), 7.24 (t, J = 7.5 Hz, 2H), 7.15 (t, J = 9.9 Hz, 4H), 6.83 (t, J = 7.4 Hz, 2H), 6.29 (d, J = 7.4 Hz, 2H). ESI−HRMS (m/z): calcd. for $[C_{48}H_{32}N_4Ir]^+$, 857.2256; found, 857.2283. Anal. Calcd for $C_{48}H_{32}F_6IrN_4P{\cdot}0.9CH_2Cl_2$: C, 54.46; H, 3.16; N, 5.20. Found: C, 54.59; H, 2.99; N, 5.31.

Photophysical and Nonlinear Transmission Measurements. The photophysical studies used spectroscopic-grade solvents, which were bought from VWR International and used as is. The UV−vis absorption and emission spectra were recorded on a Varian Cary 50 spectrophotometer and a HORIBA FluoroMax 4 fluorometer/phosphorometer, respectively. The absolute emission quantum yields (QY) of **Ir1**−**Ir10** were determined using an Ocean Optics integrating sphere (ISP-50-8-R) fiber coupled to a Delta linear-variable filter (LVF) set that was fiber coupled to a broad white LED (Sandhouse, LLS Neutral White, 4100K CCT). The set of LVFs were aligned with a modified Ocean Optics LVF mount and positioned for a narrow excitation band peaked at 450 nm. On the detection side, the integrating sphere was coupled to a bifurcated fiber cable to Ocean Optics UV−vis QE65000 and NIRQ512 spectrometers with a detection range of 350−1700 nm. For absolute QY calibration, spectral shape was corrected using the blackbody emission from a tungsten filament as a reference and QY was calibrated (±5%) against multiple samples representing five different standards with emission spanning the visible spectrum.[54,55] The samples were degassed and maintained in an oxygen-free environment prior to and during each QY measurement.

The nanosecond transient difference absorption (TA) spectra and lifetimes of **Ir1**−**Ir10** were measured on an Edinburgh LP920 laser flash photolysis spectrometer in degassed CH_3CN solutions. The excitation wavelength was 355 nm from a Nd:YAG laser with a pulse duration of 4.1 ns and a repetition rate of 1 Hz. Prior to each measurement, the sample solution was degassed with N_2 for 40 min. The triplet excited-state molar extinction coefficients (ε_T) at the TA band maxima were determined by the singlet depletion method.[56] A benzene solution of SiNc (ε_{590} = 70 000 M^{-1} cm^{-1}, Φ_T = 0.20)[57] was utilized as a reference for determination of the triplet excited-state quantum yield through the relative actinometry method.[58]

The nonlinear transmission measurement followed the procedure reported in our previous work.[59]

Computational Methods. Density functional theory (DFT) and linear response time-dependent DFT (TDDFT) calculations of **Ir1**−**Ir10** were carried out using Gaussian 09 software package.[60] Optimization of the ground state and calculations of the excited states were conducted using the B3LYP[61] functional with the basis set of LANL2DZ for Ir,[62] and 6-31g* for H, C, and N.[63] Solvent effects were included via Conductor Polarized Continuum Model (CPCM)[64,65] for dichloromethane.

The theoretical absorption spectra were generated by computing the lowest 125 singlet excitations from the ground state singlet equilibrium geometry, and the resulting transition energies and oscillator strengths were broadened via eq 2 in ref 66, with a line width of 0.12 eV to model the thermal broadening of optical bands to be comparable to experimental spectra. The emission of complexes **Ir1**−**Ir10** was

DOI: 10.1021/acs.inorgchem.8b03162
Inorg. Chem. XXXX, XXX, XXX−XXX

simulated using TDDFT ΔSCF approach, which computed the phosphorescence energy by calculating the triplet excited state transitions using TDDFT based on the triplet equilibrium geometry.[32] The nature of the triplet and singlet transitions were characterized by computing the natural transition orbitals (NTOs)[67] via Gaussian09 and visualized using VMD with 0.02 isovalue.[68]

■ RESULTS AND DISCUSSION

Electronic Absorption. The absorption spectra of complexes **Ir1**−**Ir10** were measured in different solvents at room temperature. Figure 1 displays the spectra in dichloromethane, and Table 1 lists the absorption band maxima and molar extinction coefficients. The normalized absorption spectra in other solvents are presented in Figure S1 of the Supporting Information. These spectra generally can be divided into four regions: the high-energy, strong absorbing band(s) below 310 nm; the structured medium-energy bands at ca. 310−400 nm; the lower-energy featureless band at ca. 400−500 nm; and the very weakly absorbing band(s) between 500 and 600 nm. According to the shape of these absorption bands and the corresponding molar extinction coefficients, these bands can be attributed to the ligand-localized $^1\pi,\pi^*$ transitions, the dominant $^1\pi,\pi^*$ transitions mixed with charge transfer (^{1}CT, i.e., metal-to-ligand charge transfer (^{1}MLCT)/ligand-to-ligand charge transfer (^{1}LLCT)) transitions, the ^{1}MLCT/^{1}LLCT/^{1}ILCT (intraligand charge transfer) transitions, and the mixed ^{1,3}MLCT/^{1,3}LLCT transitions, respectively. These assignments are in accord with those reported for the other biscyclometalated Ir(III) complexes,[18,19,27,69] and are verified by the TDDFT calculation results (see NTOs in the Supporting Information, Tables S1−S3).

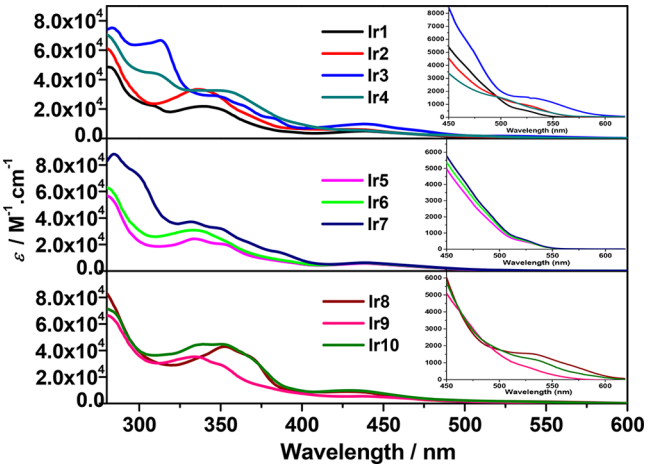

Figure 1. Room-temperature UV−vis absorption spectra of **Ir1**−**Ir10** in CH_2Cl_2. The insets are the expanded spectra in the region of 450−625 nm.

Examination of the lowest-energy absorption bands (500−600 nm) of complexes **Ir1**−**Ir10** found that benzannulation at the 5,6-position of pyridine (**Ir2** vs **Ir1**), 6,7-position of quinoline (**Ir3** vs **Ir2**), 5,6- and 5′,6′-position of 2,2′-bipyridine (**Ir8** vs **Ir1**), and 3,4- and 3′,4′-position of 2,2′-bipyridine (**Ir10** vs **Ir1**) gave rise to a red-shift of the ^{1,3}MLCT/^{1,3}LLCT absorption bands with an increased molar extinction coefficient in comparison to their corresponding parent complexes. On the other hand, benzannulation at the 7,8-position of quinoline (**Ir4** vs **Ir2**), 4,5- and 4′,5′-position of 2,2′-bipyridine (**Ir9** vs **Ir1**), or 2,2′,3,3′-position of 2,2′-bipyridine (**Ir5** vs **Ir1**) essentially did not impact the energy of the ^{1,3}MLCT/^{1,3}LLCT absorption

Table 1. Photophysical Data for Ir1−Ir10

	λ_{abs}/nm (log ε)[a]	λ_{em}/nm (τ_{em}/μs); Φ_{em}[b]	k_r/s^{-1}[c,d]	k_{nr}/s^{-1}[c,d]	$\lambda_{T1\text{-}Tn}$/nm (τ_{TA}/μs; log $\varepsilon_{T1\text{-}Tn}$); Φ_T[e]
Ir1	281 (4.68), 307 (4.35), 339 (4.34), 440 (3.73), 519 (2.79)	553 (2.16); 0.41	1.90×10^5	2.73×10^5	407 (2.14; −), 573 (2.13, −), 783 (−; −); −[g]
Ir2	280 (4.79), 337 (4.52), 433 (3.84), 518 (3.02)	613 (0.52); 0.081	1.56×10^5	1.77×10^6	380 (0.30; −), 782 (0.33; −); −[g]
Ir3	280 (4.85), 307 (4.65), 351 (4.51), 436 (3.76), 523 (3.20)	738 (2.62); 0.0031	1.18×10^3	3.80×10^5	339 (−,−), 390 (3.42; −), 555 (3.32; −), 660 (3.47; −); −[g]
Ir4	283 (4.87), 312 (4.82), 347 (4.46), 438 (3.99), 500 (3.18)	583 (−[f]); 0.0022	−	−	398 (4.52; −), 555 (4.44; −), 795 (4.46; −); −[g]
Ir5	280 (4.75), 333 (4.38),, 350 (4.31), 438 (3.77), 518 (2.73)	554 (2.77); 0.71	2.56×10^5	1.05×10^5	363 (−; −), 407 (2.82; −), 578 (2.93; −), 797 (2.87; −); −[g]
Ir6	281 (4.79), 333 (4.49), 439 (3.78), 518 (2.79)	553 (2.71); 0.78	2.88×10^5	8.12×10^4	360 (−; −), 407 (2.79; −), 575 (2.81; −), 797 (2.79; −); −[g]
Ir7	284 (4.94), 331 (4.57), 348 (4.51), 439 (3.79), 518 (2.85)	554 (31.0); 0.27	8.71×10^3	2.35×10^4	412 (sh., 19.6; −), 475 (19.6; −); −[g]
Ir8	280 (4.91), 352 (4.63), 365 (4.56), 430 (3.96), 527 (3.19)	645 (1.00); 0.084	1.56×10^5	1.70×10^6	390 (0.61; −), 449 (0.63; −), 641 (0.63; 4.35), 782 (0.63; 4.64); 0.54
Ir9	280 (4.82), 334 (4.55), 350 (4.47), 437 (3.75), 517 (2.96)	582 (−[f]); 0.0013	−	−	741 (0.04; −); −[g]
Ir10	280 (4.85), 339 (4.65), 350 (4.65), 431 (3.99), 529 (3.10)	651 (0.49); 0.075	5.47×10^5	6.74×10^6	533 (0.25; 4.42), 695 (0.25; 4.40); 0.28

[a] λ_{abs} and ε refer to the absorption band maxima and molar extinction coefficients of electronic absorption in CH_2Cl_2, respectively. [b] Room-temperature emission band maxima (λ_{em}) and lifetimes (τ_{em}) in CH_2Cl_2 ($c = 1 \times 10^{-5}$ mol/L). The quantum yields were measured using a fiber-coupled Ocean Optics integrating sphere with λ_{ex} = 450 nm. Emission signals in the wavelength range of 380−820 nm were integrated for all of the complexes except for **Ir3**. The integration range for **Ir3** was 380−900 nm. [c,d] Radiative decay rates (k_r) and nonradiative decay rates (k_{nr}) calculated by $k_r = \Phi_{em}/(\Phi_T\tau_{em})$ and $k_{nr} = (1\text{-}\Phi_{em})/(\Phi_T\tau_{em})$, respectively. For **Ir8** and **Ir10**, the estimated triplet quantum yields (Φ_T) from the TA measurement were used. For the other complexes, Φ_T was assumed to be 1. [e] $\lambda_{T1\text{-}Tn}$, τ_{TA}, $\varepsilon_{T1\text{-}Tn}$, and Φ_T are the nanosecond TA band maxima, triplet excited state lifetimes, triplet extinction coefficients, and triplet quantum yields, respectively, in degassed CH_3CN solutions. [f] The emission signal was too weak to allow the lifetime to be measured. [g] The $\varepsilon_{T1\text{-}Tn}$ values cannot be estimated using the singlet depletion method because of the lack of a bleaching band in these complexes. The Φ_T values thus cannot be determined, either.

DOI: 10.1021/acs.inorgchem.8b03162
Inorg. Chem. XXXX, XXX, XXX−XXX

Table 2. NTOs of the Transitions Contributing to the S_1 States of Complexes Ir1−Ir10 in CH_2Cl_2

	S_1 State	Hole	Electron		S_1 State	Hole	Electron
Ir1	485 nm $f = 0.002$	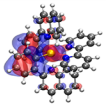	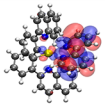	**Ir6**	483 nm $f = 0.000$	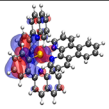	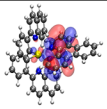
Ir2	517 nm $f = 0.004$	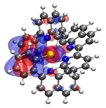	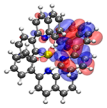	**Ir7**	482 nm $f = 0.000$	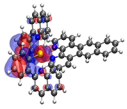	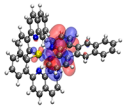
Ir3	560 nm $f = 0.002$	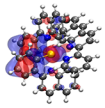	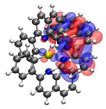	**Ir8**	537 nm $f = 0.010$	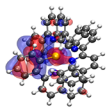	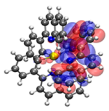
Ir4	487 nm $f = 0.025$	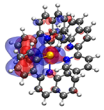	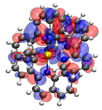	**Ir9**	461 nm $f = 0.004$	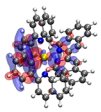 56% 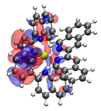 20%	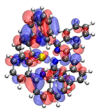 56% 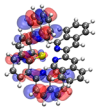 20%
Ir5	483 nm $f = 0.001$	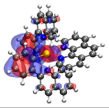	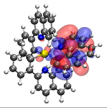	**Ir10**	556 nm $f = 0.002$	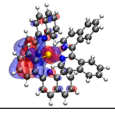	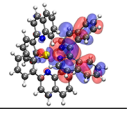

band compared to their corresponding parent complex. In addition, fusing a phenyl or a naphthyl ring to the 5,6-position of 1,10-phenanthroline did not affect the energies of the ^{1,3}MLCT/^{1,3}LLCT transitions in **Ir6** and **Ir7** compared to their parent complex **Ir5**.

The site-dependent benzannulation effect was more clearly evidenced in the calculated S_1 state energies for these complexes. As listed in Table 2, benzannulation at the 5,6-/5′,6′-position or 3,4-/3′,4′-position of 2,2′-bipyridine stabilized the S_1 states in complexes **Ir2**, **Ir8**, and **Ir10**, respectively, compared to the S_1 state of their parent complex **Ir1**, while benzannulation at the 4,5-/4′,5′-positions of 2,2′-bipyridine destabilized the S_1 state in **Ir9** in comparison to that of **Ir1**. In contrast, benzannulation at the 2,2′,3,3′-position 2,2′-bipyridine and further benzannulation at phenanthroline essentially had no impact on the S_1 state energies of **Ir5**−**Ir7** compared to that of **Ir1**. While benzannulation at the 6,7-position of quinoline lowered the S_1 state in **Ir3**, benzannulation at the 7,8-position of quinoline raised the S_1 state in **Ir4**. This trend matched well with experimental observations and was in accordance with that reported by our group earlier for another series of cyclometalated monocationic Ir(III) complexes with different C^N ligands.[32]

The DFT calculation showed that the HOMO → LUMO transition was the dominant contributor (∼70%) to the S_1 states of all of the complexes except for **Ir9** (see Supporting Information, Table S4). Electron density distribution plots of the HOMOs and LUMOs in **Ir1**−**Ir10** (Table S4) clearly demonstrated that the HOMOs of these complexes were predominantly distributed on the phenyl rings of the 2-phenylquinoline ligands and the d-orbital of the Ir(III) center, while the LUMOs were exclusively localized on the diimine ligand. Thus, benzannulation at the diimine ligand would mainly impact the LUMO energies. As depicted in Figure 2, the ground-state MO energy diagram for **Ir1**−**Ir10** manifested that

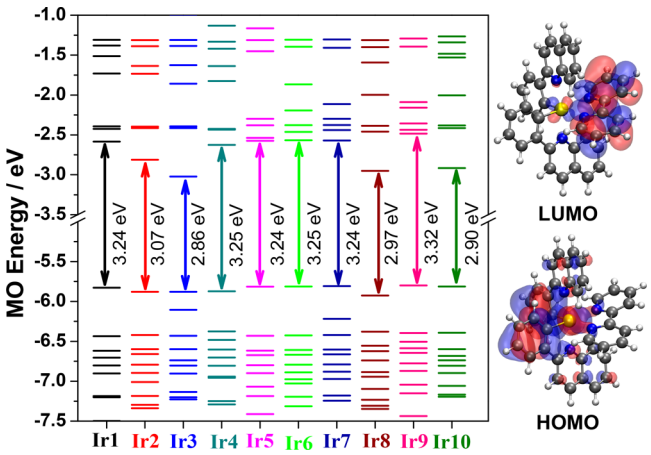

Figure 2. Ground-state molecular orbital diagram for **Ir1**−**Ir10** in CH_2Cl_2 (HOMO and LUMO of **Ir1** are plotted as representative).

benzannulation drastically changed the LUMO energies but had a minor effect on the HOMO energies. Benzannulation at the 5,6-/5′,6′-position or 3,4-/3′,4′-position of 2,2′-bipyridine or at the 6,7-position of quinoline significantly stabilized the LUMOs in complexes **Ir2**, **Ir3**, **Ir8**, and **Ir10**, whereas benzannulation at the other sites of 2,2′-bipyridine or the 7,8-position of quinoline either did not affect or slightly raised the LUMOs in **Ir4**−**Ir7** and **Ir9** compared to that of **Ir1**.

According to Thompson/Gordon's work[38] and our previous work,[32] benzannulation on the diimine ligand can be regarded as the interaction between the LUMO of the parent compound and the HOMO or LUMO of *cis*-1,3-butadiene or ethene, relying on the symmetry of MO at the benzannulation site. As shown in Figure 3, when benzannulation took place at the 5,6-position of one of the pyridine rings, the symmetry of the **Ir1** LUMO at this site was consistent with the *cis*-1,3-butadiene LUMO symmetry

DOI: 10.1021/acs.inorgchem.8b03162
Inorg. Chem. XXXX, XXX, XXX−XXX

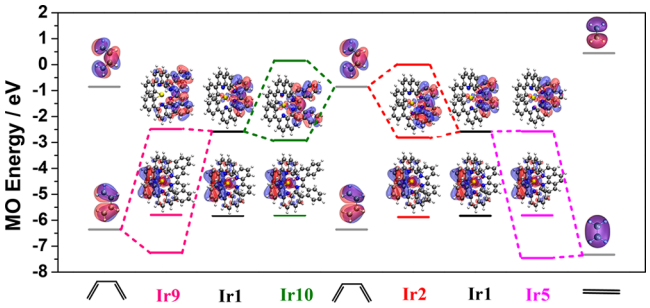

Figure 3. Frontier molecular orbital mixing between *cis*-1,3-butadiene or ethene and parent molecules.

and led to a LUMO−LUMO interaction. The LUMO−LUMO interactions resulted in a stabilized LUMO in **Ir2** and thus the red-shifted CT absorption band in its UV−vis absorption spectrum compared to that of **Ir1**. Similarly, the symmetry of the LUMO of **Ir1** at the 5,6-/5′,6′-position and the 3,4-/3′,4′-position of 2,2′-bipyridine matched the *cis*-1,3-butadiene LUMO symmetry, resulting in stabilized LUMOs and red-shifted CT absorption bands in complexes **Ir8** (Supporting Information Figure S3) and **Ir10** (Figure 3). In contrast, benzannulation at the 4,5-/4′,5′-position of 2,2′-bipyridine led to an HOMO−LUMO interaction due to the matched symmetry of the *cis*-1,3-butadiene HOMO and the **Ir1** LUMO at these positions. Such an interaction gave rise to a destabilized LUMO in complex **Ir9** and enlarged the HOMO−LUMO energy gap, which consequently resulted in a blue-shifted CT absorption band. From complex **Ir1** to **Ir5**, benzannulation at the 2,2′,3,3′-position of 2,2′-bipyridine in **Ir1** can be considered as the interaction between the LUMO of **Ir1** and the HOMO of ethene due to symmetry matching requirement. Such an interaction showed a negligible impact on the LUMO of **Ir5** and essentially did not affect the CT transition in **Ir5** compared to that of **Ir1**. A similar MO symmetry analysis was applied to the other complexes, and the results are presented in Figure S3 of the Supporting Information.

Photoluminescence. To evaluate the site-dependent benzannulation effect on the triplet excited states of complexes **Ir1**−**Ir10**, the emission characteristics of these complexes were studied at room temperature in different solvents. The emission spectra in CH_2Cl_2 are shown in Figure 4, and the emission lifetimes and quantum yields in CH_2Cl_2 are tabulated in Table 1.

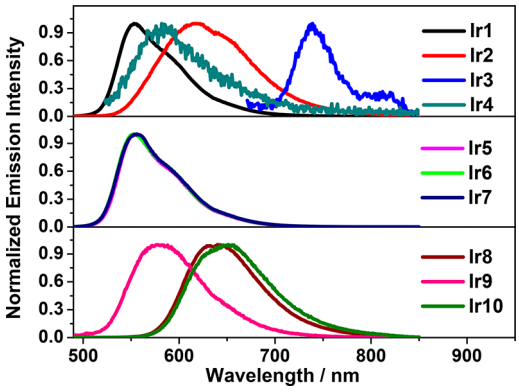

Figure 4. Normalized emission spectra of **Ir1**−**Ir10** in CH_2Cl_2 at room temperature. (λ_{ex} = 438 nm for **Ir1**, 430 nm for **Ir2**, 439 nm for **Ir3**, 436 nm for **Ir4**, 438 nm for **Ir5**, 437 nm for **Ir6**, 440 nm for **Ir7**, 428 nm for **Ir8**, 436 nm for **Ir9**, and 437 nm for **Ir10**.

The excitation spectra of **Ir1**−**Ir10** in CH_2Cl_2 monitored at their respective emission band maxima are presented in Figure S4 of the Supporting Information. The normalized emission spectra and emission parameters in other solvents are given in Figure S5 and Table S5 of the Supporting Information, respectively. The emission of these complexes was sensitive to oxygen quenching and was moderately long-lived (0.49−31.0 μs) (except for the very weakly emissive **Ir4** and **Ir9**, in which the signals were too low to be detected), indicating the phosphorescent nature of the emission. These features are in agreement with the other Ir(III) complexes reported in the literature.[17−19,24−33,39−42] Except for **Ir3**, exhibited emission in the near-IR region with clear vibronic structures, the emission of all of the other complexes were broad and almost featureless.

In comparison to the parent complex **Ir1**, benzannulation at the 3,4-/3′,4′-position, 4,5-/4′,5′-position, or 5,6-/5′,6′-position of 2,2′-bipyridine all induced a bathochromic shift of the emission spectra in **Ir2**, **Ir8**, **Ir9**, and **Ir10**, accompanied by a shortened lifetime and a reduced emission quantum yield, while benzannulation at the 2,2′,3,3′-position of 2,2′-bipyridine essentially had no impact on the emission energy of **Ir5**, but with a slightly longer lifetime and an increased emission quantum yield. A drastically red-shifted emission into the NIR region was observed for **Ir3** after fusion of one more phenyl ring at the 6,7-position of quinoline in **Ir2**. On the contrary, benzannulation at the 7,8-position of quinoline in **Ir2** induced a salient blue-shift of the emission of **Ir4** and a lower quantum yield compared with those of **Ir2** and **Ir3**. Going from **Ir5** to **Ir7**, further extending the π-conjugation along the 5,6-position of 1,10-phenanthroline did not alter the emission energies of complexes **Ir6** and **Ir7**. However, the emission lifetime of **Ir7** was over an order of magnitude longer than those of **Ir5** and **Ir6**, but its emission quantum yield is less than half of those for **Ir5** and **Ir6**. Similar to the trend discovered for the S_1 states in these complexes based on the electronic absorption, the site-dependent benzannulation influenced the lowest triplet excited state (T_1) energies in a similar manner, but the impact is more pronounced on the T_1 state than on the S_1 state.

To understand the electronic configurations of the emitting states for **Ir1**−**Ir10**, TDDFT calculations were performed, and the NTOs representing the emitting T_1 states are displayed in Table 3. The trend of the calculated emission energies matched the trend of the experimental energies very well (Supporting Information Figure S6). For complexes **Ir1**, **Ir2**, **Ir5**−**Ir7**, their holes are almost exclusively distributed on the phenyl rings of the C^N ligands and on the metal d-orbital; however, the electrons are localized on the diimine ligands and the d-orbital. Therefore, the emitting states in these complexes are predominantly attributed to the ^{3}MLCT/^{3}LLCT states, mixed with some ^{3}LMCT/^{3}d,d configurations. For complex **Ir3**, both the hole and electron are almost exclusively on the benzoquinoline part of the N^N ligand, mixed with a minor contribution from the metal d-orbitals. This indicates the dominant $^3\pi,\pi^*$ nature with minor ^{3}d,d character for the emitting state in **Ir3**. The NTOs show that the emitting state of **Ir9** also has predominant $^3\pi,\pi^*$ configuration with minor ^{3}d,d contribution. However, both the hole and electron are mainly distributed on one of the C^N ligands. The remaining complexes **Ir4**, **Ir8** and **Ir10** all have holes on the phenyl rings of the C^N ligands and the d-orbitals, with some contributions from the N^N ligands, while their electrons are distributed on the N^N ligands and the d-orbitals. Therefore, the emitting states in these complexes have mixed ^{3}MLCT/^{3}LLCT/$^3\pi,\pi^*$ configurations with minor

DOI: 10.1021/acs.inorgchem.8b03162
Inorg. Chem. XXXX, XXX, XXX−XXX

Table 3. NTOs Representing the Lowest Triplet Transitions (T_1) of Ir1−Ir10 in CH_2Cl_2

	T_1/nm	Hole	Electron		T_1/nm	Hole	Electron
Ir1	625	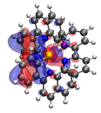	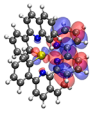	**Ir6**	606	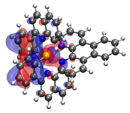	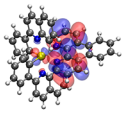
Ir2	659	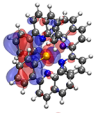	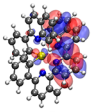	**Ir7**	610	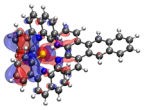	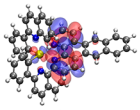
Ir3	1146	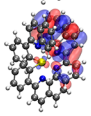	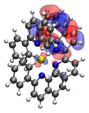	**Ir8**	733	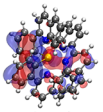	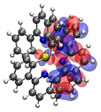
Ir4	647	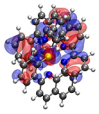	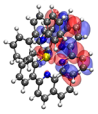	**Ir9**	647	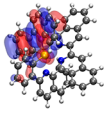	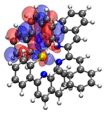
Ir5	600	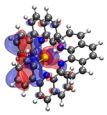	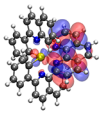	**Ir10**	744	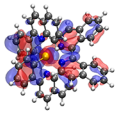	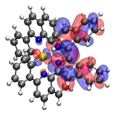

contribution from the ^{3}LMCT/^{3}d,d configurations. It is noted that the electrons in **Ir5**−**Ir7** are only localized on the phenanthroline motif, and they did not extend to the additional phenyl ring(s). Therefore, the emission energies in these three complexes are essentially the same.

For complexes **Ir1**, **Ir2**, **Ir8**, and **Ir10**, which have dominant charge transfer configurations in their emitting states, benzannulation reduced the energies of their emitting states, which significantly increased the nonradiative decay rate constants (see k_{nr} in Table 1) in **Ir2**, **Ir8**, and **Ir10** compared with that in **Ir1** without pronouncedly altering their radiative decay rate constants (k_r). This trend is in accord with the energy gap law.[70,71] For complexes **Ir5** and **Ir6**, they have the similar k_rs to that of **Ir1**, but their k_{nr}s are smaller than that of **Ir1**. The reduced k_{nr}s in **Ir5** and **Ir6** can be attributed to the rigidity of phenanthroline and its derivatives compared with bipyridine. Consequently, their emission quantum yields are higher than that of **Ir1**. Interestingly, the emission energy and the T_1 state configuration of **Ir7** resemble those of **Ir5** and **Ir6**, but its lifetime is an order of magnitude longer than those of **Ir5** and **Ir6**, and its emission quantum yield is less than half the values for **Ir5** and **Ir6**. Examination of the triplet energy diagram obtained from the TDDFT calculation (Supporting Information Figure S7) reveals that unlike the other complexes, the second triplet excited state (T_2) in **Ir7** lies closely to its T_1 state, which makes it possible to be configurationally mixed with T_1 state and reaches an equilibrium. Because the T_2 state of **Ir7** has a $^3\pi,\pi^*$ configuration (Supporting Information Table S6), admixing T_2 with T_1 drastically reduces the k_r and k_{nr} in **Ir7** compared with those in **Ir5** and **Ir6**, which dramatically prolongs the emission lifetime of **Ir7**. Complex **Ir4** also has a significant charge transfer character in its emitting T_1 state, but its emission quantum yield is very low. This could presumably be attributed to its more distorted geometry from the octahedral configuration in its ground and excited states due to its more sterically hindered N^N ligand,[32] which could drastically increase the k_{nr} and consequently reduce the emission quantum yield in **Ir4**.

Transient Absorption (TA). The nanosecond TA of complexes **Ir1**−**Ir10** in acetonitrile was investigated to further clarify their triplet excited state characteristics. The TA spectra of **Ir1**−**Ir10** immediately after laser excitation are shown in Figure 5, and the time-resolved TA spectra are presented in

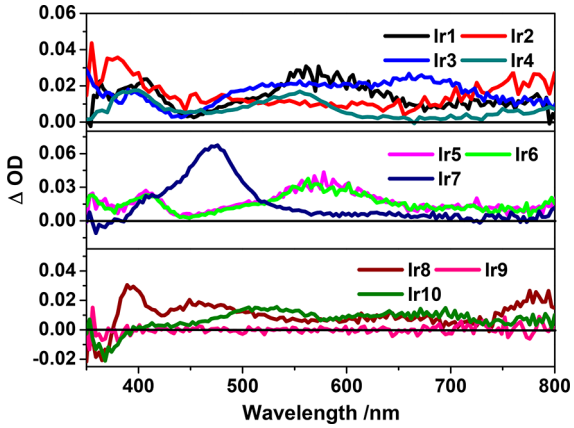

Figure 5. Nanosecond transient differential absorption spectra of complexes **Ir1**−**Ir10** in acetonitrile solution at zero delay after excitation (A_{355} = 0.4 in a 1 cm cuvette, λ_{ex} = 355 nm).

Supporting Information Figure S8. The TA band maxima, triplet excited-state lifetimes, triplet extinction coefficients and quantum yields (when applicable), are listed in Table 1. The triplet excited-state lifetimes extrapolated from the decay profiles of the TA signals resembled the lifetimes obtained from the decay of emission in acetonitrile (see Supporting Information Table S5). Accordingly, we can tentatively assign the transient absorbing excited states to the emitting excited states except for **Ir7**.

The TA spectra in Figure 5 and the data in Table 1 manifested that **Ir1**, **Ir5**, and **Ir6** possessed identical TA spectra, and their triplet lifetimes were on the same order. The TA spectral feature of **Ir4** appeared to resemble those of **Ir1**, **Ir5**, and **Ir6** but was somewhat blue-shifted accompanied by a longer lifetime. The TA spectra of **Ir2** and **Ir8** were similar in shape, but the TA band maximum was red-shifted for **Ir8** compared with **Ir2**, and the lifetime of **Ir8** is longer than that of **Ir2**. The TA spectra of **Ir3**

DOI: 10.1021/acs.inorgchem.8b03162
Inorg. Chem. XXXX, XXX, XXX−XXX

and **Ir10** were similar in the region of 450−800 nm with very broad and moderately strong absorption. However, the triplet lifetime of **Ir3** is 1 order of magnitude longer than that of **Ir10**, suggesting the different parentages of the T_1 states in these two complexes. In addition, the spectra of **Ir2**, **Ir3**, **Ir4**, and **Ir8** all resembled those of their corresponding Ir(III) complexes bearing the same N^N ligand but differing in the C^N ligands.[32] Considering the natures of the T_1 states in these complexes (discussed in the Photoluminescence section) and comparing these spectra to those of their corresponding N^N ligands and those of their Zn^{2+} perturbed ligands (Supporting Information Figure S9), we attribute the observed TA to ^{3}MLCT/^{3}LLCT states for **Ir1**, **Ir2**, **Ir5**, and **Ir6**, to N^N localized $^3\pi,\pi^*$ states for **Ir3** and **Ir7**, to $^3\pi,\pi^*$/^{3}MLCT/^{3}LLCT state for **Ir4**, and to ^{3}MLCT/^{3}LLCT/$^3\pi,\pi^*$ states for **Ir8** and **Ir10**. No TA signals were observed from **Ir9**, which is consistent with the C^N ligand localized $^3\pi,\pi^*$ nature for its T_1 state because we reported earlier that neither 2-phenylquinoline (pq) nor its chloro-bridged dinuclear Ir(III) precursor $[(Ir(pq)_2Cl]_2$ produced any TA signals.[31] The drastically different TA spectra and lifetimes of **Ir8**, **Ir9**, and **Ir10** clearly manifested the distinct effects that variations of the benzannulation site at the N^N ligand exerted on the triplet excited-state absorption.

Complex **Ir7** exhibited a quite distinct TA spectrum from the other complexes, with a very strong absorption band at 475 nm and a quite long triplet lifetime. This TA spectral feature was identical to that of its N^N ligand (see Supporting Information Figure S9). Therefore, the observed TA for **Ir7** is ascribed to the $^3\pi,\pi^*$ state localized on the N^N ligand. As discussed in the previous section, the T_2 state in **Ir7** has the N^N ligand localized $^3\pi,\pi^*$ configuration and is energetically closed to its T_1 state. Thus, it can configurationally mix with the T_1 state and predominantly contribute to the TA of **Ir7**.

Reverse Saturable Absorption. The results and discussions in the previous sections revealed that the ground- and excited-state absorption and the triplet lifetimes were affected remarkably by the site of benzannulation at the N^N ligand in complexes **Ir1**−**Ir10**. In addition, the TA signals for all complexes except for **Ir9** were positive at 532 nm upon 355 nm excitation, implying a stronger excited-state absorption at this wavelength compared to that of the ground state. This phenomenon set up the condition for reverse saturable absorption (RSA, a nonlinear absorption in which the increased incident fluence enhances the absorptivity of a compound) to occur. To demonstrate the RSA, nonlinear transmission measurement for all complexes was performed in acetonitrile solutions in a 2 mm cuvette using the 532 nm 4.1 ns laser pulses as the light source. For convenient comparison, the linear transmission of each sample solution at 532 nm in the 2 mm cuvette was adjusted to 80%. The resultant nonlinear transmission curves are presented in Figure 6. With increased incident energy, the transmission of all complexes decreased pronouncedly, implying the appearance of RSA. The RSA strength decreased following the sequence of **Ir7** > **Ir5** ≈ **Ir6** ≈ **Ir1** > **Ir3** > **Ir2** > **Ir10** > **Ir4** > **Ir8** > **Ir9**, with **Ir7** exhibiting the strongest RSA by reducing the transmission from 80% to 25% at the incident energy of 709 μJ. The RSA trend matched well with their ΔOD values at 532 nm (see Table 4). It should be noted that the TA spectra shown in Figure 5 were obtained upon a 355 nm excitation. With the assumption that the initially populated singlet excited state upon the 355 nm excitation rapidly decayed to the lowest singlet excited state and then converted to the T_1 state via ISC, the triplet excited state generated via the 355 or 532 nm excitation should be the same T_1 state. This notion was partially supported by the identical emission energies obtained upon excitation at the $^1\pi,\pi^*$/^{1}CT band in the UV region and at the ^{1}CT band in the blue spectral region (see the exemplified emission spectra of **Ir5** upon 333 and 438 nm excitations in Figure S10 of the Supporting Information). In such a case, the trends of the ΔOD values deduced from Figure 5 for 355 nm excitation can be assumed to be the same as the ΔOD value trends upon 532 nm excitation.

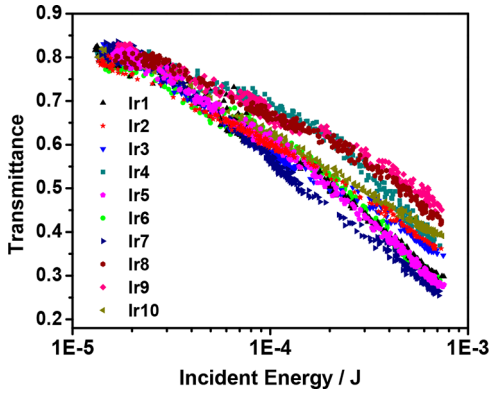

Figure 6. Nonlinear transmission curves for **Ir1**−**Ir10** at a 80% of linear transmittance in 2 mm cuvette (in acetonitrile solution) using the 532 nm 4.1 ns laser pulses. The beam radius at the focal point was approximately 96 μm.

It is well-known that the RSA strength is mainly determined by the ratio of the excited-state absorption cross section vs that of the ground-state (σ_{ex}/σ_0) at the interested wavelength. A decreased ground-state absorption and/or increased excited-state absorption would induce a strong RSA. The σ_0 values can be deduced from the molar extinction coefficients at 532 nm using the conversion equation $\sigma = 2303\varepsilon/N_A$ (where N_A is the Avogadro's constant). Unfortunately, the σ_{ex} values for most of the complexes could not be obtained because of the lack of obvious bleaching bands in the TA measurement so that the singlet depletion method was unable to be applied to estimate the ε_{ex} values. Nevertheless, the ΔOD values that measure the difference between the excited-state and ground-state absorption can serve as a good indicator for the strength of the excited-state absorption. A general trend is that the complexes with larger ground-state absorption at 532 nm due to benzannulation (i.e., **Ir2**, **Ir4**, **Ir8**, **Ir9**, and **Ir10**) exhibited weaker excited-state absorption at 532 nm. The combination of these changes reduced the RSA strength for these complexes. Although **Ir3** had an increased σ_0 value at 532 nm, its much stronger excited-state absorption at this wavelength counteracted the increased ground-state absorption and consequently gave rise to a stronger RSA than **Ir2**, **Ir4**, **Ir8**, **Ir9**, and **Ir10**.

■ CONCLUSIONS

Ten biscyclometalated Ir(III) complexes featuring various N^N ligands were synthesized, and their ground- and excited-state properties were systematically studied. Extending π-conjugation of the N^N ligand via benzannulation induced either a bathochromic or hypsochromic shift in their absorption and emission spectra compared to their corresponding parent complex. This phenomenon was explained by analyzing the molecular orbital symmetry at the benzannulation site via DFT calculations. Relying on the benzannulation site, stabilization

DOI: 10.1021/acs.inorgchem.8b03162
Inorg. Chem. XXXX, XXX, XXX−XXX

Table 4. Ground-State Absorption Cross Sections (σ_0) and ΔOD Values of Ir1−Ir10 at 532 nm

	1	2	3	4	5	6	7	8	9	10
$\sigma_0/10^{-18}$ cm^2	1.39	3.06	5.65	2.47	1.28	1.37	1.52	5.80	2.42	4.61
ΔOD[b]	0.018	0.011	0.020	0.014	0.020	0.020	0.024	0.007	–[c]	0.015

[a]Measured in CH_2Cl_2. [b]Measured in CH_3CN. [c]Too weak to be measured.

(when benzannulation occurred at the 3,4-/3′,4′-position or 5,6-/5′,6′-position of 2,2′-bipyridine ligand or at the 6,7-position of the quinoline ring of the N^N ligand) or destabilization (when benzannulation took place at the 4,5-/4′,5′-position of 2,2′-bipyridine ligand or at the 7,8-position of the quinoline ring on the N^N ligand) or no change (when benzannulation occurred at the 2,2′,3,3′-position of 2,2′-bipyridine or 5,6-position of phenanthroline ligand) of the LUMO was found upon interaction with *cis*-1,3-butanediene or ethene. Consequently, a narrowed or enlarged or identical HOMO−LUMO gap was produced compared to the parent complex and a red- or blue-shifted, or no-change charge transfer absorption band was observed. Similar trends were observed in the emission spectra of these complexes. The site of benzannulation also impacted the ns TA of these complexes drastically. Because of the site-dependent benzannulation effects on the ground- and excited-state absorption, RSA strength of these complexes at 532 nm also varied, which followed the trend of **Ir7** > **Ir5** ≈ **Ir6** ≈ **Ir1** > **Ir3** > **Ir2** > **Ir10** > **Ir4** > **Ir8** > **Ir9**. This trend correlated well with their ΔOD values at 532 nm and their ground-state absorption cross sections at 532 nm. Benzannulation that increased ground-state absorption but reduced the excited-state absorption resulted in reduced RSA, while benzannulation that had a minor impact on the ground-state absorption but increased the excited-state absorption gave rise to enhanced RSA. A detailed understanding of the benzannulation site-dependent bathochromic or hypsochromic shift of the absorption and emission spectra is vital for designing organometallic complexes with predetermined photophysical properties for applications in OLEDs, dye-sensitized solar cells, phosphorescent probes, and photosensitizers for upconversion or photodynamic therapy.

■ ASSOCIATED CONTENT

Supporting Information

The Supporting Information is available free of charge on the ACS Publications website at DOI: 10.1021/acs.inorgchem.8b03162.

The NTOs representing transitions contributing to the major absorption bands in **Ir1**−**Ir10**; the HOMOs and LUMOs electron density distribution plots of **Ir1**−**Ir10**; comparison of the experimental and theoretical UV−vis absorption and emission spectra of **Ir1**−**Ir10** in CH_2Cl_2; MO mixing for complexes **Ir3**, **Ir4**, and **Ir8**; triplet excited state energy diagram; normalized UV−vis absorption and emission spectra in different solvents; the time-resolved TA spectra of **Ir1**−**Ir10** and their diimine ligands and $ZnCl_2$ complexes in CH_3CN; emission spectrum of **Ir5** using different excitation wavelengths; and the full author list for ref 60 (PDF)

■ AUTHOR INFORMATION

Corresponding Author

*E-mail: Wenfang.Sun@ndsu.edu. Telephone: 701-231-6254. Fax: 701-231-8831.

ORCID

Bingqing Liu: 0000-0002-1540-2235
Erik K. Hobbie: 0000-0001-6158-8977
Svetlana Kilina: 0000-0003-1350-2790
Wenfang Sun: 0000-0003-3608-611X

Notes

The authors declare no competing financial interest.

■ ACKNOWLEDGMENTS

We are grateful to the National Science Foundation (DMR-1411086 and CHE-1800476) for the financial support for complex synthesis, photophysical studies, and DFT calculations. S.K. acknowledges the Center for Computationally Assisted Science and Technology (CCAST) at the North Dakota State University for providing the computational resources and administrative support. S.K. also thanks the Sloan Research Fellowship BR2014-073 for partial financial support for acquiring the quantum chemistry software.

■ REFERENCES

(1) Dixon, I. M.; Collin, J.−P.; Sauvage, J.−P.; Flamigni, L.; Encinas, S.; Barigelletti, F. A Family of Luminescent Coordination Compounds: Iridium(III) Polyimine Complexes. *Chem. Soc. Rev.* **2000**, *29*, 385−391.

(2) Goldsmith, J. I.; Hudson, W. R.; Lowry, M. S.; Anderson, T. H.; Bernhard, S. Discovery and High−Throughput Screening of Heteroleptic Iridium Complexes for Photoinduced Hydrogen Production. *J. Am. Chem. Soc.* **2005**, *127*, 7502−7510.

(3) Zhao, J.; Wu, W.; Sun, J.; Guo, S. Triplet Photosensitizers: from Molecular Design to Applications. *Chem. Soc. Rev.* **2013**, *42*, 5323−5351.

(4) Holder, E.; Langeveld, B. M. W.; Schubert, U. S. New trends in the use of transition metal−ligand complexes for applications in electroluminescent devices. *Adv. Mater.* **2005**, *17*, 1109−1121.

(5) King, K. A.; Spellane, P. J.; Watts, R. J. Excited−state Properties of a Triply Ortho−metalated Iridium(III) Complex. *J. Am. Chem. Soc.* **1985**, *107*, 1431−1432.

(6) Goswami, S.; Sengupta, D.; Paul, N. D.; Mondal, T. K.; Goswami, S. Redox Non−Innocence of Coordinated 2−(Arylazo) Pyridines in Iridium Complexes: Characterization of Redox Series and an Insight into Voltage−Induced Current Characteristics. *Chem. - Eur. J.* **2014**, *20*, 6103−6111.

(7) Radwan, Y. K.; Maity, A.; Teets, T. S. Manipulating the Excited States of Cyclometalated Iridium Complexes with β−Ketoiminate and β−Diketiminate Ligands. *Inorg. Chem.* **2015**, *54*, 7122−7131.

(8) Müllen, K.; Scherf, U. *Organic Light−Emitting Devices*; Wiley−VCH: Weinheim, Germany, 2006.

(9) Mao, H.−T.; Zang, C.−X.; Shan, G.−G.; Sun, H.−Z.; Xie, W.−F.; Su, Z.−M. Achieving High Performances of Nondoped OLEDs Using Carbazole and Diphenylphosphoryl−Functionalized Ir(III) Complexes as Active Components. *Inorg. Chem.* **2017**, *56*, 9979−9987.

(10) Xu, H.; Chen, R.; Sun, Q.; Lai, W.; Su, Q.; Huang, W.; Liu, X. Recent Progress in Metal−Organic Complexes for Optoelectronic Applications. *Chem. Soc. Rev.* **2014**, *43*, 3259−3302.

(11) Wang, Y.; Wang, S. M.; Ding, J. Q.; Wang, L. X.; Jing, X. B.; Wang, F. S. Dendron Engineering in Self−Host Blue Iridium Dendrimers Towards Low−Voltage−Driving and Power−Efficient Nondoped Electrophosphorescent Devices. *Chem. Commun.* **2017**, *53*, 180−183.

DOI: 10.1021/acs.inorgchem.8b03162
Inorg. Chem. XXXX, XXX, XXX−XXX

(12) Mydlak, M.; Bizzarri, C.; Hartmann, D.; Sarfert, W.; Schmid, G.; De Cola, L. Positively Charged Iridium(III) Triazole Derivatives as Blue Emitters for Light−Emitting Electrochemical Cells. *Adv. Funct. Mater.* **2010**, *20*, 1812−1820.
(13) Sunesh, C. D.; Mathai, G.; Choe, Y. Constructive Effects of Long Alkyl Chains on the Electroluminescent Properties of Cationic Iridium Complex−based Light−Emitting Electrochemical Cells. *ACS Appl. Mater. Interfaces* **2014**, *6*, 17416−17425.
(14) McKenzie, L. K.; Sazanovich, I. V.; Baggaley, E.; Bonneau, M.; Guerchais, V.; Williams, J. A. G.; Weinstein, J. A.; Bryant, H. E. Metal Complexes for Two−Photon Photodynamic Therapy: A Cyclometallated Iridium Complex Induces Two−Photon Photosensitization of Cancer Cells under Near−IR Light. *Chem. - Eur. J.* **2017**, *23*, 234−238.
(15) Stacey, O. J.; Pope, S. J. A. New Avenues in the Design and Potential Application of Metal Complexes for Photodynamic Therapy. *RSC Adv.* **2013**, *3*, 25550−25564.
(16) Maggioni, D.; Galli, M.; D'Alfonso, L.; Inverso, D.; Dozzi, M. V.; Sironi, L.; Iannacone, M.; Collini, M.; Ferruti, P.; Ranucci, E.; D′Alfonso, G. *Inorg. Chem.* **2015**, *54*, 544−−553.
(17) Li, Y.; Dandu, N.; Liu, R.; Li, Z.; Kilina, S.; Sun, W. Effects of Extended π−Conjugation in Phenanthroline (N^N) and Phenylpyridine (C^N) Ligands on the Photophysics and Reverse Saturable Absorption of Cationic Heteroleptic Iridium(III) Complexes. *J. Phys. Chem. C* **2014**, *118*, 6372−6384.
(18) Liu, R.; Dandu, N.; Chen, J.; Li, Y.; Li, Z.; Liu, S.; Wang, C.; Kilina, S.; Kohler, B.; Sun, W. Influence of Different Diimine (N^N) Ligands on the Photophysics and Reverse Saturable Absorption of Heteroleptic Cationic Iridium(III) Complexes Bearing Cyclometalating 2−{3−[7−(Benzothiazol−2−yl)fluoren−2−yl]phenyl}−pyridine (C^N) Ligands. *J. Phys. Chem. C* **2014**, *118*, 23233−23246.
(19) Sun, W.; Pei, C.; Lu, T.; Cui, P.; Li, Z.; McCleese, C.; Fang, Y.; Kilina, S.; Song, Y.; Burda, C. Reverse Saturable Absorbing Cationic Iridium(III) Complexes Bearing the 2−(2−Quinolinyl) quinoxaline Ligand: Effects of Different Cyclometalating Ligands on Linear and Nonlinear Absorption. *J. Mater. Chem. C* **2016**, *4*, 5059−5072.
(20) Lang, X.; Zhao, J.; Chen, X. Cooperative Photoredox Catalysis. *Chem. Soc. Rev.* **2016**, *45*, 3026−3038.
(21) Huo, H.; Wang, C.; Harms, K.; Meggers, E. Enantioselective, Catalytic Trichloromethylation through Visible−Light−Activated Photoredox Catalysis with a Chiral Iridium Complex. *J. Am. Chem. Soc.* **2015**, *137*, 9551−9554.
(22) Huo, H.; Shen, X.; Wang, C.; Zhang, L.; Röse, P.; Chen, L.−A.; Harms, K.; Marsch, M.; Hilt, G.; Meggers, E. Asymmetric Photoredox Transition−Metal Catalysis Activated by Visible Light. *Nature* **2014**, *515*, 100−−103.
(23) Chen, Y.; Guan, R.; Zhang, C.; Huang, J.; Ji, L.; Chao, H. Two−Photon Luminescent Metal Complexes for Bioimaging and Cancer Phototherapy. *Coord. Chem. Rev.* **2016**, *310*, 16−40.
(24) Okada, S.; Okinaka, K.; Iwawaki, H.; Furugori, M.; Hashimoto, M.; Mukaide, T.; Kamatani, J.; Igawa, S.; Tsuboyama, A.; Takiguchi, T.; Ueno, K. Substituent Effects of Iridium Complexes for Highly Efficient Red OLEDs. *Dalton Trans.* **2005**, No. 9, 1583−1590.
(25) Nazeeruddin, Md. K.; Wegh, R. T.; Zhou, Z.; Klein, C.; Wang, Q.; De Angelis, F.; Fantacci, S.; Grätzel, M. Efficient Green−Blue−Light−Emitting Cationic Iridium Complex for Light−Emitting Electro−Chemical Cells. *Inorg. Chem.* **2006**, *45*, 9245−9250.
(26) Skorka, L.; Filapek, M.; Zur, L.; Małecki, J. G.; Pisarski, W.; Olejnik, M.; Danikiewicz, W.; Krompiec, S. Highly Phosphorescent Cyclometalated Iridium(III) Complexes for Optoelectronic Applications: Fine Tuning of the Emission Wavelength through Ancillary Ligands. *J. Phys. Chem. C* **2016**, *120*, 7284−7294.
(27) Zhao, Q.; Liu, S.; Shi, M.; Wang, C.; Yu, M.; Li, L.; Li, F.; Yi, T.; Huang, C. Series of New Cationic Iridium(III) Complexes with Tunable Emission Wavelength and Excited State Properties: Structures, Theoretical Calculations, and Photophysical and Electrochemical Properties. *Inorg. Chem.* **2006**, *45*, 6152−6160.
(28) Zeng, X.; Tavasli, M.; Perepichka, I. F.; Batsanov, A. S.; Bryce, M. R.; Chiang, C.−J.; Rothe, C.; Monkman, A. P. Cationic Bis−Cyclometallated Iridium(III) Phenanthroline Complexes with Pendant Fluorenyl Substituents: Synthesis, Redox, Photophysical Properties and Light−Emitting Cells. *Chem. - Eur. J.* **2008**, *14*, 933−−943.
(29) Kim, K.−Y.; Farley, R. T.; Schanze, K. S. An Iridium(III) Complex that Exhibits Dual Mechanism Nonlinear Absorption. *J. Phys. Chem. B* **2006**, *110*, 17302−−17304.
(30) Li, Y.; Dandu, N.; Liu, R.; Hu, L.; Kilina, S.; Sun, W. Nonlinear Absorbing Cationic Iridium(III) Complexes Bearing Benzothiazolylfluorene Motif on the Bipyridine (N^N) Ligand: Synthesis, Photophysics and Reverse Saturable Absorption. *ACS Appl. Mater. Interfaces* **2013**, *5*, 6556−6570.
(31) Wang, L.; Cui, P.; Kilina, S.; Sun, W. Towards Broadband Reverse Saturable Absorption: Investigating the Impact of Cyclometalating Ligand π−Conjugation on the Photophysics and Reverse Saturable Absorption of Cationic Heteroleptic Iridium Complexes. *J. Phys. Chem. C* **2017**, *121*, 5719−5730.
(32) Liu, B.; Lystrom, L.; Kilina, S.; Sun, W. Tuning the Ground State and Excited State Properties of Monocationic Iridium(III) Complexes by Varying the Site of Benzannulation on Diimine Ligand. *Inorg. Chem.* **2017**, *56*, 5361−5370.
(33) Wang, C.; Lystrom, L.; Yin, H.; Hetu, M.; Kilina, S.; McFarland, S. A.; Sun, W. Increasing the Triplet Lifetime and Extending The Ground−State Absorption Of Biscyclometalated Ir(III) Complexes for Reverse Saturable Absorption and Photodynamic Therapy Applications. *Dalton Trans.* **2016**, *45*, 16366−16378.
(34) Adachi, M.; Murata, Y. Relationship between π−Conjugation Size and Electronic Absorption Spectrum: Novel π−Conjugation Size Dependence of Indoaniline Dyes. *J. Phys. Chem. A* **1998**, *102*, 841−845.
(35) Adachi, M.; Nagao, Y. Design of Near−Infrared Dyes Based on π−Conjugation System Extension 2. Theoretical Elucidation of Framework Extended Derivatives of Perylene Chromophore. *Chem. Mater.* **2001**, *13*, 662−669.
(36) Martin, N.; Segura, J. L.; Seoane, C. Design and Synthesis of TCNQ and DCNQI Type Electron Acceptor Molecules as Precursors for ′Organic Metals′. *J. Mater. Chem.* **1997**, *7*, 1661−1676.
(37) Jensen, B. S.; Parker, V. D. Reactions of Aromatic Anion Radicals and Dianions. II. Reversible Reduction of Anion Radicals to Dianions. *J. Am. Chem. Soc.* **1975**, *97*, 5211−5217.
(38) Hanson, K.; Roskop, L.; Djurovich, P. I.; Zahariev, F.; Gordon, M. S.; Thompson, M. E. A Paradigm for Blue− or Red−Shifted Absorption of Small Molecules Depending on the Site of π−Extension. *J. Am. Chem. Soc.* **2010**, *132*, 16247−16255.
(39) Li, Z.; Cui, P.; Wang, C.; Kilina, S.; Sun, W. Nonlinear Absorbing Cationic Bipyridyl Iridium(III) Complexes Bearing Cyclometalating Ligands with Different Degrees of π − Conjugation: Synthesis, Photophysics, and Reverse Saturable Absorption. *J. Phys. Chem. C* **2014**, *118*, 28764−28775.
(40) Zhu, X.; Cui, P.; Kilina, S.; Sun, W. Multifunctional Cationic Iridium(III) Complexes Bearing 2−Aryloxazolo[4,5−f][1,10]-phenanthroline (N^N) Ligand: Synthesis, Crystal Structure, Photophysics, Mechanochromic/Vapochromic Effects, and Reverse Saturable Absorption. *Inorg. Chem.* **2017**, *56*, 13715−13731.
(41) Pei, C.; Cui, P.; McCleese, C.; Kilina, S.; Burda, C.; Sun, W. Heteroleptic Cationic Iridium (III) Complexes Bearing Naphthalimidyl Substituents: Synthesis, Photophysics and Reverse Saturable Absorption. *Dalton Trans.* **2015**, *44*, 2176−2190.
(42) Li, Z.; Li, H.; Gifford, B. J.; Peiris, W. D. N.; Kilina, S.; Sun, W. Synthesis, Photophysics, and Reverse Saturable Absorption of 7−(Benzothiazol−2−yl)−9,9−di(2−ethylhexyl)−9H− Fluoren−2−yl Tethered $[Ir(bpy)(ppy)_2]PF_6$ and $Ir(ppy)_3$ Complexes (bpy = 2,2′−Bipyridine, ppy = 2−Phenylpyridine). *RSC Adv.* **2016**, *6*, 41214−41228.
(43) Xiang, H.; Chen, H.; Tham, H. P.; Phua, S. Z. F.; Liu, J.−G.; Zhao, Y. Cyclometalated Iridium(III)−Complex−Based Micelles for Glutathione−Responsive Targeted Chemotherapy and Photodynamic Therapy. *ACS Appl. Mater. Interfaces* **2017**, *9*, 27553−−27562.
(44) Ma, D.−L.; Leung, C.−H.; Zhong, H.−J.; He, B.. Method of Detecting Helicase Activity. U.S. Patent US20170145472A1, May 25, 2017.

DOI: 10.1021/acs.inorgchem.8b03162
Inorg. Chem. XXXX, XXX, XXX−XXX

(45) Yang, H.; P.-Y. Ma, V.; S.-H. Chan, D.; He, H.−Z.; Leung, C.−H.; Ma, D.−L. A Cyclometallated Iridium(III) Complex As a c−myc G−Quadruplex Stabilizer and Down−Regulator of c−myc Oncogene Expression. *Curr. Med. Chem.* **2013**, *20*, 576−−582.
(46) Li, A. H.; Beard, D. J.; Coate, H.; Honda, A.; Kadalbajoo, M.; Kleinberg, A.; Sherman, D.; Laufer, R.; Mulvihill, K.; Nigro, A.; et al. One−Pot Friedländer Quinoline Synthesis: Scope and Limitations. *Synthesis* **2010**, *2010*, 1678−1686.
(47) Karim, M.; Jahng, Y. Unusual Product Distribution from Friedlander Reaction of Di− and Tri−Acetylbenzenes with 3−Aminonaphthalene−2−carbaldehyde and Properties of New Benzo-[g]quinoline−derived Aza−aromatics. *Molecules* **2014**, *19*, 12842−12851.
(48) Riesgo, E. C.; Hu, Y.−Z.; Bouvier, F.; Thummel, R. P.; Scaltrito, D. V.; Meyer, G. J. Crowded Cu(I) Complexes Involving Benzo[h]-quinoline: π−Stacking Effects and Long−Lived Excited States. *Inorg. Chem.* **2001**, *40*, 3413−3422.
(49) Verhoeven, J. W.; Van, D. T. E. B.; Steemers, F. J.; Verboom, W.; Reinhoudt, D. N.; Hofstraat, J. W. Complex Comprising Rare Earth Metal Ion and Complexing Moiety for Optical Device. PCT Int. Appl., 9849163, Nov 05, 1998.
(50) Lu, W.; Vicic, D. A.; Barton, J. K. Reductive and Oxidative DNA Damage by Photoactive Platinum(II) Intercalators. *Inorg. Chem.* **2005**, *44*, 7970−7980.
(51) Nelson, T. D.; Crouch, R. D. Cu, Ni, and Pd Mediated Homocoupling Reactions in Biaryl Syntheses: The Ullmann Reaction. *Org. React.* **2004**, *63*, 265−555.
(52) Milstein, D.; Stille, J. K. Palladium−Catalyzed Coupling of Tetraorganotin Compounds with Aryl and Benzyl Halides. Synthetic Utility and Mechanism. *J. Am. Chem. Soc.* **1979**, *101*, 4992−4998.
(53) Gao, R.; Ho, D. G.; Hernandez, B.; Selke, M.; Murphy, D.; Djurovich, P. I.; Thompson, M. E. Bis−cyclometalated Ir(III) Complexes as Efficient Singlet Oxygen Sensitizers. *J. Am. Chem. Soc.* **2002**, *124*, 14828−14829.
(54) van Dam, B.; Bruhn, B.; Dohnal, G.; Dohnalová, K. Limits of Emission Quantum Yield Determination. *AIP Adv.* **2018**, *8*, No. 085313.
(55) Brouwer, A. M. Standards for Photoluminescence Quantum Yield Measurements in Solution (IUPAC Technical Report). *Pure Appl. Chem.* **2011**, *83*, 2213−2228.
(56) Carmichael, I.; Hug, G. L. Triplet−Triplet Absorption Spectra of Organic Molecules in Condensed Phases. *J. Phys. Chem. Ref. Data* **1986**, *15*, 1−250.
(57) Firey, P. A.; Ford, W. E.; Sounik, J. R.; Kenney, M. E.; Rodgers, M. A. J. Silicon Naphthalocyanine Triplet State and Oxygen. A Reversible Energy−Transfer Reaction. *J. Am. Chem. Soc.* **1988**, *110*, 7626−7630.
(58) Kumar, C. V.; Qin, L.; Das, P. K. Aromatic Thioketone Triplets and Their Quenching Behaviour Towards Oxygen and Di−t−butylnitroxy Radical. A Laser−Flash−Photolysis Study. *J. Chem. Soc., Faraday Trans. 2* **1984**, *80*, 783−793.
(59) Liu, B.; Lystrom, L.; Kilina, S.; Sun, W. Effects of Varying the Benzannulation Site and π-Conjugation of Cyclometalating Ligand on Photophysics and Reverse Saturable Absorption of Monocationic Iridium(III) Complexes. *Inorg. Chem.* **2019**, *58*, 476−488.
(60) Frisch, M. J.; Trucks, G. W.; Schlegel, H. B.; Scuseria, G. E.; Robb, M. A.; Cheeseman, J. R.; Scalmani, G.; Barone, V.; Mennucci, B.; Peterson, G. A.; et al. *Gaussian 09*, revision B.1; Gaussian, Inc.: Wallingford, CT, 2009.
(61) Lee, C.; Yang, W.; Parr, R. G. Development of the Colle−Salvetti correlation−energy formula into a functional of the electron density. *Phys. Rev. B: Condens. Matter Mater. Phys.* **1988**, *37*, 785−789.
(62) Hay, P. J.; Wadt, W. R. Ab initio effective core potentials for molecular calculations. Potentials for the transition metal atoms Sc to Hg. *J. Chem. Phys.* **1985**, *82*, 270−283.
(63) Adamo, C.; Barone, V. Toward reliable density functional methods without adjustable parameters: The PBE0 model. *J. Chem. Phys.* **1999**, *110*, 6158−6170.
(64) Barone, V.; Cossi, M.; Tomasi, J. Geometry optimization of molecular structures in solution by the polarizable continuum model. *J. Comput. Chem.* **1998**, *19*, 404−417.
(65) Cossi, M.; Barone, V.; Cammi, R.; Tomasi, J. Ab initio study of solvated molecules: a new implementation of the polarizable continuum model. *Chem. Phys. Lett.* **1996**, *255*, 327−335.
(66) Bjorgaard, J. A.; Sifain, A. E.; Nelson, T.; Myers, T. W.; Veauthier, J. M.; Chavez, D. E.; Scharff, R. J.; Tretiak, S. Two−photon absorption in conjugated energetic molecules. *J. Phys. Chem. A* **2016**, *120*, 4455−4464.
(67) Martin, R. L. Natural transition orbitals. *J. Chem. Phys.* **2003**, *118*, 4775−4777.
(68) Humphrey, W.; Dalke, A.; Schulten, K. VMD−Visual Molecular Dynamics. *J. Mol. Graphics* **1996**, *14*, 33−38.
(69) Wu, S.−H.; Ling, J.−W.; Lai, S.−H.; Huang, M.−J.; Cheng, C. H.; Chen, I.−C. Dynamics of the Excited States of $[Ir(ppy)_2bpy]^+$ with Triple Phosphorescence. *J. Phys. Chem. A* **2010**, *114*, 10339−10344.
(70) Caspar, J. V.; Kober, E. M.; Sullivan, B. P.; Meyer, T. J. Application of the Energy Gap Law to the Decay of Charge-Transfer Excited States. *J. Am. Chem. Soc.* **1982**, *104*, 630−632.
(71) Caspar, J. V.; Meyer, T. J. Application of the Energy Gap Law to Nonradiative, Excited-State Decay. *J. Phys. Chem.* **1983**, *87*, 952−957.

DOI: 10.1021/acs.inorgchem.8b03162
Inorg. Chem. XXXX, XXX, XXX−XXX